Available online at https://link.springer.com/journal/42241
http://www.jhydrodynamics.com
Journal of Hydrodynamics, 2019, 31(1): 137-144
https://doi.org/10.1007/s42241-019-0018-0

Multi-objective optimization of a flow straightener in a large capacity firefighting water cannon *

Qing-jiang Xiang[1, 2], Lin Xue[1, 3], Kwang-Yong Kim[2], Zhe-fu Shi[1]
1. *National Research Centre of Pumps, Jiangsu University, Zhenjiang 212013, China*
2. *Department of Mechanical Engineering, Inha University, Incheon, Korea*
3. *Shanghai Fire Research Institute of Ministry of Emergency Management, Shanghai 200032, China*

(Received May 16, 2016, Revised June 10, 2017, Accepted June 19, 2017, Published online January 23, 2019)
©China Ship Scientific Research Center 2019

Abstract: In the present study, a multi-objective optimization of a flow straightener in a firefighting water cannon is performed by using the surrogate modeling and a hybrid multi-objective genetic algorithm to increase the jet range of the water cannon. Based on analysis using the three-dimensional Reynolds-averaged Navier-Stokes equations, the optimization is carried with a surrogate model and the radial basis neural network. Three geometric design variables, i.e., the length, the thickness of the blade, and the radius of the outer pipe of the flow straightener, are selected for the optimization. The pressure drop through the water cannon and the area-averaged turbulent kinetic energy at the outlet of the water cannon, which are closely related to the jet range of the water cannon, are selected as the objective functions to be minimized. The design space is determined through a parametric study, and the Latin hypercube sampling method is used to select the design points in the design space. The Pareto-optimal solutions are obtained through the optimization. Five representative Pareto-optimal solutions are selected to study the trade-off between two objectives.

Key words: Firefighting water cannon, multi-objective optimization, surrogate model, turbulence kinetic energy, hydraulic loss

Introduction

The firefighting water cannon with a large capacity and a long jet range can be used to extinguish the fire far away[1-2]. The water cannons are used in many key fire prevention areas, such as the areas near the oil storage tank[3] and the refining equipment, the firefighting ship, the offshore oilfield guarding ship, the patrol ship, and the loading dock where the LNG and the oil are transported.

The worm and gear rotary devices are installed along with the pipes for the function of pitching and turning of the water cannon. The nozzle serves for the energy conversion from the pressure to the kinetic energy. The flow straightener is usually installed in the tube of the water cannon to eliminate the swirl and impose a fully developed velocity profile. The proper structure of a large capacity firefighting water cannon was not well studied. Hatton et al.[4] tested different nozzle shapes, with the best one for the trajectory simulation. Theobald[5] studied the stability of the water jets discharging into the air with nozzles of nominal diameter of 12.7 mm , various internal profiles and contraction angles. They focused more on nozzles, and less on the water cannon's flow straightener. It was reported that the proper design of the flow straightener improves the maximal range of the water cannon by about 5-10% as compared with the case without the flow straightener. This conclusion was supported by the experiment shows that the range is increased from 62 m to 67 m for the PS50 firefighting monitor at the working pressure of 0.8 MPa , and by Yuan et al.[6] whose experimental study shows that the range increased 3.2% after the guide vane installed in water cannon.

The flow straightener is used in fire branch, irrigation sprinkler, wind tunnel[7], chimney, and in front of the flow meter[8], etc.. The flow straighteners have various cross section shapes, such as inner fin shape, square crossing shape, triangular shape, and bullet shape. Most of them are suitable for only small diameter pipes. However, if the diameter of the water cannon's tube is large, in order to eliminate the swirl,

* Project supported by the National Natural Science Foundation of China (Grant No. 51379090).
Biography: Qing-jiang Xiang (1974-), Male, Ph. D., Associate Professor
Corresponding author: Qing-jiang Xiang,
E-mail: xiang_qj@163.com

it is better to divide the cross section of the tube into many small cells.

The length of the flow straightener is one of the important parameters in the design of the water cannon, as a conclusion made by Drainy et al.[9] who studied how the length of the Zanker plate affects the flow field in front of a flow meter. The location of the flow straightener also affects the performance. A new type of flow straightener is going to be applied in the large capacity firefighting water cannon shown in Fig. 1, which is designed with two coaxial pipes and radial blades. Bacchi and Scarabino[10] designed the similar structure of this flow straightener which is used in a chimney. Although his conclusions are drawn from the air flow, it may be applied for the water cannon as well. Xiang et al.[11-12] studied this flow straightener by using the orthogonal method, and suggested a suitable length of the flow straightener for the water cannon, and it is indicated that the thickness of the flow straightener has a significant effect on the hydraulic loss. For different application purposes, the performance of the flow straightener is represented by different parameters. For example, to reduce the measurement error of the flow meter, Laribi et al.[13] studied the etoile flow straightener, recommended in the standard ISO 5167, and used the velocity profiles and the turbulence intensity to compare with the fully developed pipe flow. To get better spray performance of the impact sprinkler, Yan et al.[14] studied the bullet shape flow straightener, by using the hydraulic loss and the discharge coefficient to characterize the performance.

The multi-objective optimization based on the 3-D computational fluid dynamics (CFD) analysis is widely applied in many engineering designs. The multi-objective optimization methods for engineering applications were reviewed by Marler and Arora[15]. A surrogate model was proposed as the approximation of an objective function, and was found to be effective to reduce the computing time in the optimization process.

The surrogate based optimization was widely used to develop efficient designs in various applications. Queipo et al.[16] presented a comprehensive discussion of the fundamental issues in the surrogate-based analysis and optimization, with a liquid rocket injector design as an example. Samad et al.[17] studied the predictive capabilities of different surrogate models, such as the response surface approximation (RSA), the kriging (KRG), and the radial basis neural networks (RBNN), for the optimization of a transonic axial compressor blade. Afzal and Kim[18-19] used the RSA and RBNN surrogate models for a multi-objective optimization of the micromixers. In their study, the mixing index and the pressure loss were selected as the objective functions, and the Pareto-optimal front representing the trade-off among the objectives was obtained by using the multi-objective genetic algorithm (MOGA).

As mentioned above, some investigations were focused on the flow straightener of the water cannon, but without any attempt to optimize the structure of the straightener so far. In this study, a multi-objective optimization of the flow straightener is performed to optimize the two objective functions, i.e., the pressure drop and the turbulent kinetic energy at the outlet of the canon with three geometric design variables. The turbulent kinetic energy is assumed to affect the jet range of the water cannon. 3-D Reynolds averaged Navier-Stokes (RANS) equations combined with a turbulence closure model are solved to determine the objective functions. The optimization is carried out by coupling the RBNN surrogate model with a hybrid MOGA.

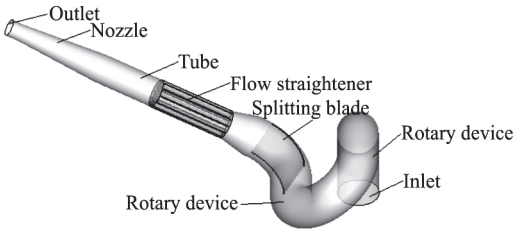

Fig. 1(a) Flow passage of firefighting water cannon

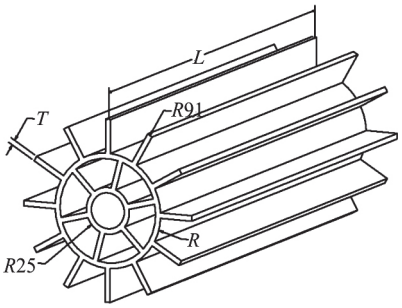

Fig. 1(b) Structure of flow straightener

1. Flow in water cannon

The firefighting water cannon considered in this work is composed of nozzle, tube, flow straightener, splitting blade, and rotary devices, as shown in Fig. 1(a). A detailed schematic diagram of the flow straightener is shown in Fig. 1(b). In Fig. 1(b), $R25$ means the radius of the inner pipe, which is 25 mm, R represents the radius of the outer pipe of the flow straightener, and $R91$ means the radius of the tube, which is 91 mm, and where the flow straightener is installed. The following design variables are selected for the optimization, i.e., the length of the flow straightener (L), the thickness of the blades (T),

and the radius of the outer pipe (R). The flow rate of the water cannon is designed as 1 500 m^3/h, the length of the tube is 900 mm, and the diameter of the nozzle at the outlet is approximately 100 mm.

The commercial CFD software, ANSYS FLUENT[20], is used for the flow analysis. The numerical analysis is carried out by solving the steady 3-D RANS equations through a finite volume solver. The standard k-ε turbulence model is suitable for the high Reynolds number turbulent flow and is adopted in the current analysis. The governing equations include equations of the continuity, the momentum conservation, the turbulence kinetic energy and its dissipation rate. As shown in Fig. 1(a), the whole computational domain of the water cannon is divided into three parts. Two interfaces are set at the planes where the water enters and leaves the flow straightener. A hexahedral grid system is used to discretize the computational domain as shown in Fig. 2.

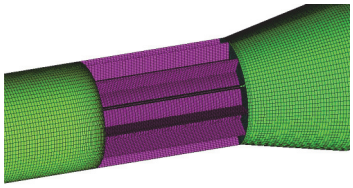

Fig. 2 (Color online) Hexahedral grids of the flow straightener

For the boundary conditions, a uniform velocity is imposed at the inlet of the water cannon. The inlet turbulence condition is specified as 10% of the turbulent intensity. The static pressure is set as zero at the outlet. No-slip adiabatic boundary conditions are applied on the walls. For the pressure-velocity coupling, the SIMPLE scheme is selected. As the standard wall function is used, the first grid points from a wall are located at y^+ with a value greater than 155[11]. The convergence criterion for monitoring residuals is of order of 10^{-5}. Approximately ten thousand iterations are required for the solution to converge.

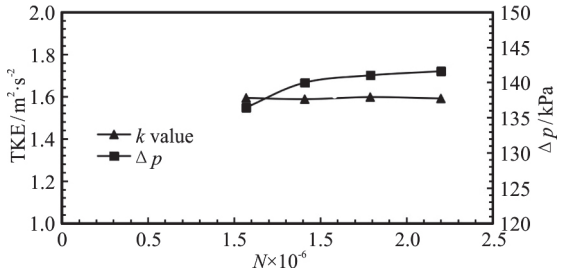

Fig. 3 Grid independency test

With the number of the total grid nodes in a range from 10^6 to 2.3×10^6, a grid independency test is performed for the pressure drop and the turbulent kinetic energy (TKE) at the outlet as shown in Fig. 3. According to the results shown in Fig. 3, the grid with approximately 1.8×10^6 nodes is used for further calculations.

2. Design variables and objective functions

Three design variables shown in Fig. 1(b) are selected for the optimization: the length of the flow straightener (L), the thickness of the blades (T) and the radius of the outer pipe (R). The design variables and their ranges are shown in Table 1, where the reference values with subscript 0 are used to normalize the variables. $L_0 = 900$ mm is the total length of the tube where the flow straightener is installed, $R_0 = 91$ mm is the radius of the tube, and $T_0 = 25$ mm is a reference thickness which is equal to the radius of the inner pipe.

Table 1 Design variables and ranges

Design variables	L/L_0	T/T_0	R/R_0
Lower bound	0.08	0.10	0.4
Upper bound	0.80	0.22	0.8

In order to build the surrogate model, some design (or experimental) points are required for building the design space. The Latin hypercube sampling (LHS) method is an effective sampling method to select these design points. Twenty-seven design points are selected for the three design variables in this paper. The LHS provides many distinct levels in the design space for the design points. These levels are spaced evenly from the lower bound to the upper bound of the design space to insure that all portions of the design space are represented.

As the given example in introduction of this paper, the performance of the flow straightener can be represented by the hydraulic loss, the swirl of the flow, the outlet turbulent kinetic energy, the discharge coefficient and so on. Thus, the objective functions are selected among these performance parameters. To achieve the longest range of the water jet, the hydraulic loss in the water cannon should be reduced, and thus the pressure drop between the inlet and the outlet of the water cannon is selected as one of the objective functions. High turbulent intensity at the outlet of the water cannon may disturb the stability of the water jet, and then make the jet disperse in the air earlier. Therefore, it is assumed that a smaller turbulent kinetic energy at the outlet produces a longer jet range. With this assumption, the relationship between the turbulent kinetic energy and the jet range plays a very important role, fortunately, it is observed

through the experiment that the water cannon has the largest turbulent kinetic energy and the shortest jet range in the case without the flow straightener. Thus, the turbulent kinetic energy at the exit of the water cannon is selected as one of the objective functions. The relationship between the jet range and the water swirl at the outlet needs a further investigation. The discharge coefficient shows the ability of the fluids passing through the water cannon under the same inlet pressure condition, so that is considered having the same effect as the hydraulic loss to be selected as the objective function.

As described above, two objective functions, F_k, F_p are employed to optimize the flow straightener of the water cannon:

$$F_k = \frac{k_{\text{ave}}}{k_0} \tag{1}$$

$$F_p = \frac{\Delta p}{\Delta p_0} \tag{2}$$

where k_{ave} is the area-weighted average turbulent kinetic energy at the outlet of the water cannon, reflecting the effect of the turbulence on the jet range. Δp is the total pressure drop between the inlet and the outlet of the firefighting water cannon representing the hydraulic loss. k_0, Δp_0 are the reference values corresponding to the values without the flow straightener.

3. Surrogate construction and multi-objective genetic algorithm

In this work, a RBNN model is generated as a surrogate model for each objective function and a hybrid MOGA is used for the optimization. The RBNN model consists of a hidden layer of radial basis neurons and an output layer of linear neurons. A customized RBNN function, newrb, available in the MATLAB (MATLAB, 2007) for the surrogate construction, testing and validation, is used in the present study and its detailed implementation was shown in Afzal and Kim[18-19]. In particular, the performance of the RBNN function approximation depends on the network parameters, the spread constant (Sc) and the error goal (EG). Among the two parameters, the spread constant, Sc, can affect the performance of the network. Therefore, the network training is performed by adjusting the cross-validation error by changing the spread constant.

The MOGA is used to obtain the Pareto-optimal solutions using the MATLAB function, gamultiobj. For the optimization, the genetic algorithm is used to search the Pareto-optimal solutions in the feasible solution space bounded by the lower and upper bounds of the design variables. The fitness functions for the two objectives, F_k, F_p, are supplied in the vector form. A tournament selection operator with a tournament size of two is used to choose the parents for the next generation. The crossover combines two individuals (or parents) to form a new individual (or child) for the next generation, as a simulation of biological populations. The cross-over function is set for an intermediate, to create children by a random weighted average of the parents.

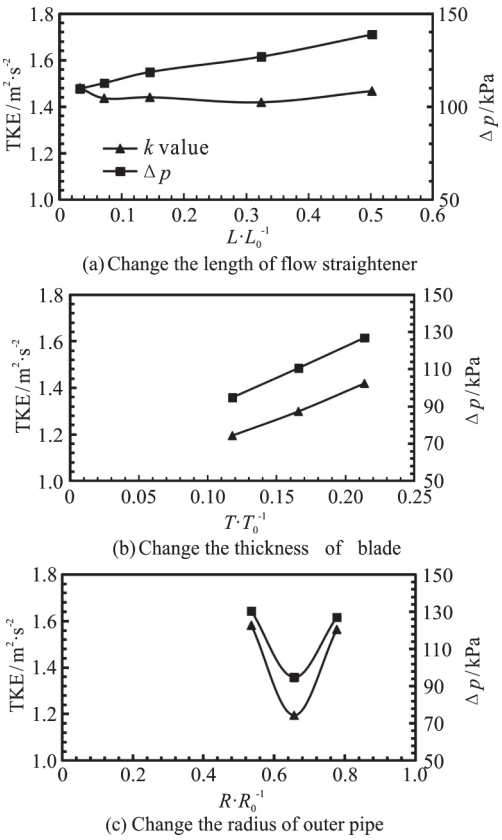

Fig. 4 Parametric study for 3 variables

The multi-objective optimization for the present problem can be formulated as follows:

Minimization of $\boldsymbol{F}(\boldsymbol{x}) = [F_1(\boldsymbol{x}), F_2(\boldsymbol{x}), F_3(\boldsymbol{x}), \cdots, F_m(\boldsymbol{x})]$

Subject to: $\mathbf{LB}_i \le \boldsymbol{x} \le \mathbf{UB}_i$, $\boldsymbol{x}$ ε R $(i = 1, 2, 3 \cdots, N)$.

where $\boldsymbol{F}(\boldsymbol{x})$ is a vector representing m real-valued objective functions, and $\boldsymbol{x}$ is a vector of N design variables. $\mathbf{LB}$, $\mathbf{UB}$ are the vectors for the lower and upper bounds of the design variables.

Global Pareto-optimal solutions are found by using the following procedures:

Step1: Choice of objective functions, design variables and ranges.

Table 2 Objective function of LHS points

No.	L/L_0	T/T_0	R/R_0	F_k	F_p
1	0.686	0.151	0.727	0.436	2.023
2	0.608	0.205	0.535	0.548	2.351
3	0.207	0.163	0.479	0.495	1.721
4	0.324	0.214	0.657	0.502	2.066
5	0.287	0.157	0.633	0.439	1.749
6	0.299	0.175	0.531	0.481	1.857
7	0.795	0.198	0.597	0.522	2.453
8	0.695	0.178	0.556	0.497	2.232
9	0.661	0.196	0.693	0.491	2.342
10	0.765	0.187	0.749	0.491	2.378
11	0.559	0.101	0.407	0.442	1.640
12	0.348	0.220	0.446	0.607	2.213
13	0.449	0.144	0.723	0.424	1.786
14	0.461	0.208	0.616	0.495	2.237
15	0.086	0.139	0.492	0.455	1.779
16	0.401	0.146	0.518	0.462	1.941
17	0.504	0.160	0.586	0.436	1.491
18	0.154	0.130	0.568	0.509	1.879
19	0.225	0.193	0.778	0.422	1.883
20	0.744	0.122	0.697	0.407	1.739
21	0.623	0.111	0.644	0.405	1.709
22	0.108	0.123	0.795	0.434	1.421
23	0.246	0.117	0.416	0.461	1.504
24	0.512	0.105	0.759	0.406	1.630
25	0.381	0.169	0.432	0.530	1.900
26	0.570	0.181	0.463	0.537	2.124
27	0.165	0.132	0.669	0.424	1.504

Step 2: Selection of design points using LHS method.

Step 3: Determination of objective function values at each design point

Step 4: Function approximation using RBNN based on the objective function values.

Step 5: Invoke gamultiobj function to obtain Pareto-optimal solutions.

Step6: Forming clusters of Pareto-optimal solutions for analysis and validation.

4. Results and discussions

Figure 4 shows the variations of the turbulent kinetic energy and the pressure drop against the selected design variables of the flow straightener; the length of the flow straightener, the thickness of the blade, and the radius of the outer pipe. In this parametric study, the reference values for the design variables are $L/L_0 = 0.342$, $T/T_0 = 0.214$ and $R/R_0 = 0.657$. Figure 4(a) shows that in a range of $L/L_0 = 0.033 - 0.502$, the pressure drop increases slowly, while the turbulence kinetic energy changes only slightly. The lower and upper bounds of L/L_0 in the design space are set to be 0.08 and 0.80, respectively, based on the results shown in Fig. 4(a). Figure 4(b) shows the effects of the thickness of the blade (T/T_0) on the performance parameters in the range of T/T_0 from 0.118 to 0.214. It is observed that both the turbulent kinetic energy and the pressure drop increase greatly with T/T_0 . The design range of T/T_0 is determined as 0.10 - 0.22 with consideration of the structure strength of the flow straightener and the national standard of the stainless steel material. Figure 4(c) shows the variations of the two objectives against the radius of the outer pipe (R/R_0) in a range from 0.536 to 0.778. Minimum values for the turbulence kinetic energy and for the pressure drop are found in this range, and the two performance parameters are also affected significantly by the radius of the outer pipe. The design range of R/R_0 is set to 0.4-0.8 based on the cross-section layout of the flow straightener.

As explained earlier, a sample size of 27 design points is used to discretize the design space. Table 2 lists the LHS generated design points and the values of the objective functions, obtained by the CFD analysis at the design points. The data set (Table 2) is used to construct the RBNN models for the objective functions. Based on the analysis, the values of the spread constant, $Sc = 0.85,\ 0.70$, are found to be appropriate for the objectives, F_k , F_p , respectively, at a fixed error goal, $\mathrm{EG} = 0.0002$.

Using the algorithm outlined in the previous section, the hybrid MOGA is used to obtain the Pareto-optimal front as shown in Fig. 5. The following parameters are set for the *gamultiobj* function: the population size is 120, the crossover fraction is 0.85, the Pareto-front population fraction is 0.90, the generations is 500, and the function tolerance is 10^{-6}. The Pareto-optimal front comprises 108 solutions and represents the optimum trade-off between the two objective functions. Because each solution is a global Pareto-optimal solution, none of these Pareto-optimal solutions is superior to the others for both objectives. It is not consistent to minimize the pressure drop while to keep the exit turbulent kinetic energy unchanged and vice-versa. As can be seen in Fig. 5, the turbulent kinetic energy is reduced at the cost of the increased pressure drop. Therefore, the choice of the designer plays an important role in selecting a Pareto-optimal solution that meets his/her requirements.

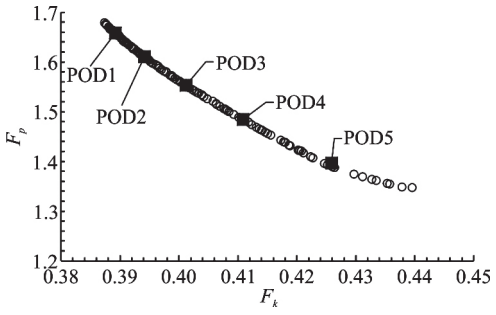

Fig.5 Pareto-optimal front for two objectcives

To analyze the variations of the objective functions against the design variables, some of the representative Pareto-optimal designs (PODs) are selected by using the K-means clustering. Also, the selected PODs are used to validate the prediction capability of the constructed RBNN model and the MOGA by comparing the optimization results predicted by the RBNN with the corresponding results from the CFD analysis. Table 3 lists the values of the design variables and the objective functions for the five PODs. The PODs 1 to 5 represent 5 different points on the Pareto-optimal front as shown in Fig. 5. As depicted in Table 3, the value of the design parameter T/T_0 is nearly constant at 0.1 (near the lower bound of its range) for all PODs, which means that the thinner blade will benefit both of the two objective functions, and this is also confirmed by Fig. 4(b). Both the pressure drop and the turbulent kinetic energy at the PODs are affected sensitively by the variations of the design variables L/L_0, R/R_0. It is observed in Table 3 that the increase of the length of the flow straightener L/L_0 lowers the turbulent kinetic energy, but increases the pressure drop. An opposite trend is observed for the design variable R/R_0. A smaller radius of the flow straightener is found to be favorable for the exit turbulent kinetic energy. With a wide range of the PODs, the designer can freely select a solution according to his needs. The optimization results are in good agreements with those of the CFD analysis. It can be deduced that the results of the construction of the RBNN model and the optimization enjoy a sufficient accuracy. The maximum error obtained is about 3.76 % (the POD 4) and 7.17 % (the POD 5) for the objective functions, F_k, F_p, respectively.

The profiles of the velocity at the outlet are plotted for three selected PODs as shown in Fig. 6. The x-axis is the radius of outlet. The velocity profile of the POD 1 is far from uniform, and looks like a sinusoidal wave with the maximum value approximately at the center of the outlet and the two local minima at ±0.03 m.This variation of the velocity profile of the POD 1 is caused by the outer pipe of the flow straightener. Compared to the POD 1, relatively smaller variation is observed in the velocity profile of the POD 2, and the variation almost disappears for the POD 5. The velocity pattern becomes uniformed due to the decreased length of the flow straightener for the POD 2 and the POD 5. The velocity profiles of the POD 3 and the POD 4 almost overlap with that of the POD 5, and for the sake of clarity, they are not shown in Fig. 6.

The turbulent kinetic energy distributions on the axis near the outlet are shown in Fig. 7 for the 5 PODs. The x-axis is the length of water cannon nozzle and the outlet is at the zero point. In the POD 1 , one sees the smallest turbulence kinetic energy level with the longest flow straightener while in the POD 5 one sees

Table 3 Validation of five optimum designs

Pareto-optimal designs (PODs)	Design variables			Objective functions				Error (%)	
				RBNN		CFD validation			
	L/L_0	T/T_0	R/R_0	F_k	F_p	F_k	F_p	F_k	F_p
1	0.72921	0.10008	0.60888	0.38925	1.65758	0.40349	1.75404	3.65	5.81
2	0.58162	0.10007	0.62651	0.39418	1.61002	0.39912	1.65258	1.25	2.64
3	0.42300	0.10005	0.64672	0.40123	1.55273	0.38937	1.53883	2.95	0.89
4	0.25303	0.10003	0.66965	0.41089	1.48384	0.39542	1.41440	3.76	4.68
5	0.10344	0.f10001	0.72349	0.42593	1.39616	0.42501	1.29595	0.21	7.17

the highest level of the turbulent kinetic energy with the shortest flow straightener near the outlet.

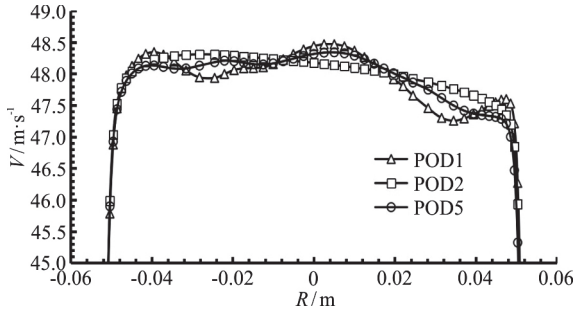

Fig.6 Profiles of the velocity at the outlet for selected PODs

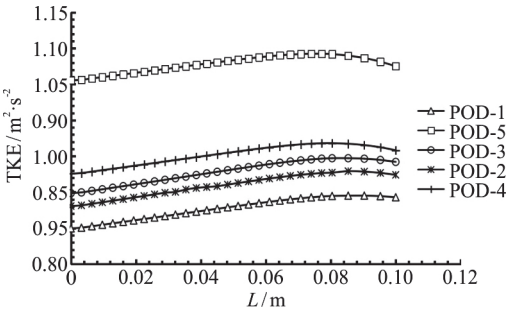

Fig.7 Turbulent kinetic energies on the axis near the outlet

5. Conclusion

In this paper, a new type of flow straightener is designed for a large capacity firefighting water cannon and investigated by using the 3-D RANS equations. A multi-objective optimization is carried out to find the optimum geometry of the flow straightener. In the optimization, a RBNN surrogate model is adopted and the MOGA is used to help designing this new flow straightener. Three design variables, i.e., the length of the flow straightener (L), the thickness of the blade (T) and the radius of the outer pipe (R) are chosen for the optimization. The objective functions are the pressure drop through the water cannon and the area-averaged turbulent kinetic energy at the outlet. The Pareto-optimal front representing the trade-off between these two objectives is obtained. The predicted optimal values in the five representative PODs, agree well with those of the CFD calculations. For the design variables in the PODs, both of the objective functions are found to decrease as T/T_0 decreases. A higher L/L_0 produces a lower turbulent kinetic energy at the exit, a larger hydraulic loss, and a larger non-uniformity of the outlet velocity profile. An opposite trend is observed for R/R_0 in the representative PODs as compared with the variable L/L_0.

Acknowledgments

This work was supported by the key science and technology project of Shanghai city (Grant No.13231203200). Thanks are also due to Dr. Arshad Afzal for helpful suggestions.

References

[1] Xin Y., Thumuluru S., Jiang F. et al. An experimental study of automatic water cannon systems for fire protection of large open spaces [J]. *Fire Technology*, 2014, 50(2): 233-248.

[2] Hsia K. H., Lien S. F., Su J. P. PTZ camera based auto-targeting control of water cannons on firefighting boats [J]. *ICIC Express Letters*, 2012, 6(3): 811-817.

[3] Miyashita T., Sugawa O., Imamura T. et al. Modeling and analysis of water discharge trajectory with large capacity monitor [J]. *Fire Safety Journal*, 2014, 63: 1-8.

[4] Hatton A. P., Leech C. M., Osborne M. J. Computer simulation of the trajectories of large water jets [J]. *International Journal of Heat and Fluid Flow*, 1985, 6(2): 137-141.

[5] Theobald C. The effect of Nozzle design on the stability and performance of turbulent water jets [J]. *Fire Safety Journal*, 1981, 4(1): 1-13.

[6] Yuan D. Q. Shi R., Cong X. Q. et al. Perfomance analysis of guide vane in long-range fire-fighting water cannon [J]. *Journal of Drainage and Irrigation Machinery Engineering*, 2017, 35(4): 333-339(in Chinese).

[7] Seo Y. J. Effect of hydraulic diameter of flow straighteners on turbulence intensity in square wind tunnel [J]. *HVAC and R Research*, 2013, 19(2): 141-147.

[8] Daev Z. A., Kairakbaev A. K. Measurement of the flow rate of liquids and gases by means of variable pressure drop flow meters with flow straighteners [J]. *Measurement Techniques*, 2017, 4: 1-5.

[9] Drainy Y. A. E., Saqr M. K., Aly H. S. et al. CFD analysis of incompressible turbulent swirling flow through zanker plate [J]. *Engineering Applications of Computational Fluid Mechanics*, 2009, 3(4): 562-572.

[10] Bacchi F., Scarabino A. Computational fluid dynamics (CFD) analysis of a flow straightener for a heater chimney [J]. *Mechanical Computational*, 2013, 19(22): 1071-1079.

[11] Xiang Q. J., Shi Z. F., Li H. Structure analysis of a new type of flow straightener used in fire fighting water cannon [C]. *The 6th International Symposium on Fluid Machinery and Fluid Engineering (ISFMFE)*, Wuhan, China, 2014.

[12] Xiang Q. J., Shi Z. F., Li H. et al. Comparative analysis of three types of straightener in long range firefighting water cannon [J]. *Journal of Drainage and Irrigation Machinery Engineering*, 2015, 33(3): 233-238.

[13] Laribi B., Youcefi A., Matene E. Length efficiency of the Etoile flow straightener numerical experimentation [C]. *Proceedings of ASME-JSME-KSME Joint Fluids Engineering Conference*, Hamamatsu, Japan, 2011.

[14] Yan H. J., Ou Y. J., Nakano K. et al. Numerical and experimental investigations on internal flow characteristic in the impact sprinkler [J]. *Irrigation and Drainage*

systems, 2009, 23(1): 11-23.
[15] Marler R. T., Arora J. S. Survey of multi-objective optimization for engineering [J]. *Structural Multidisciplinary Optimization*, 2004, 29(6): 369-395.
[16] Queipo N. V., Haftka R. T., Shyy W. et al. Surrogate-based analysis and optimization [J]. *Progress in Aerospace Sciences*, 2005, 41(1): 1-28.
[17] Samad A., Kim K. Y., Goel T. et al. Multiple surrogate modeling for axial compressor blade shape optimization [J]. *Journal of Propulsion and Power*, 2008, 24(2): 301-310.
[18] Afzat A., Kim K. Y. Multi-objective optimization of a passive micromixer based on periodic variation of velocity profile [J]. *Chemical Engineering Communications*, 2015, 202(3): 322-331.
[19] Afzat A., Kim K. Y. Multi-objective optimization of a micromixer with convergent-divergent sinusoidal walls [J]. *Chemical Engineering Communications*, 2015, 202(10): 1324-1334.
[20] FLUENT-11.0. Solver theory [M]. Canonsburg, Pennsylvania, USA: ANSYS, 2007.